X-ray absorption spectroscopy elucidates the impact of structural disorder on electron mobility in amorphous zinc-tin-oxide thin films

Sin Cheng Siah,[1,a),b)] Sang Woon Lee,[2,c)] Yun Seog Lee,[1] Jaeyeong Heo,[3] Tomohiro Shibata,[4] Carlo U. Segre,[4] Roy G. Gordon,[2] and Tonio Buonassisi[1,a)]

[1]*Massachusetts Institute of Technology, Cambridge, Massachusetts 02139, USA*
[2]*Department of Chemistry and Chemical Biology, Harvard University, Cambridge, Massachusetts 02138, USA*
[3]*Department of Materials Science and Engineering, Chonnam National University, Gwangju 500-757, South Korea*
[4]*Physics Department and CSRRI, Illinois Institute of Technology, Chicago, Illinois 606016, USA*

We investigate the correlation between the atomic structures of amorphous zinc-tin-oxide (a-ZTO) thin films grown by atomic layer deposition (ALD) and their electronic transport properties. We perform synchrotron-based X-ray absorption spectroscopy at the *K*-edges of Zn and Sn with varying [Zn]/[Sn] compositions in a-ZTO thin films. In extended X-ray absorption fine structure (EXAFS) measurements, signal attenuation from higher-order shells confirms the amorphous structure of a-ZTO thin films. Both quantitative EXAFS modeling and X-ray absorption near edge spectroscopy (XANES) reveal that structural disorder around Zn atoms increases with increasing [Sn]. Field- and Hall-effect mobilities are observed to decrease with increasing structural disorder around Zn atoms, suggesting that the degradation in electron mobility may be correlated with structural changes. © *2014 AIP Publishing LLC*. [http://dx.doi.org/10.1063/1.4884115]

Amorphous metal-oxide semiconductors (AMOS) have attracted attention for transparent optoelectronic applications including liquid-crystal displays and transparent conducting oxides for organic light-emitting diodes. Zinc oxide and related oxide classes are investigated due to their high electron mobilities compared to conventional amorphous silicon. Nomura *et al.* demonstrated high-performance flexible transistors using amorphous indium-gallium-zinc-oxide (a-IGZO) with electron mobilities exceeding 10 cm^2/V·s.[1] The high mobility and amorphous structure of AMOS enable a faster operation of the devices and elimination of grain-boundary related defects, respectively.[2,3] The high electron mobility in the amorphous state originates from the conduction band, which mainly consists of unoccupied Ns ($N \geq 5$) orbitals of metal atoms such as In-5s in a-IGZO.[4–6] The spherical symmetry of the s orbitals makes them less prone to form traps and scattering centers when the metal-oxygen-metal bonds are distorted by rotation of metal-oxygen polyhedrons.

Amorphous zinc-tin-oxide (a-ZTO) is recently highlighted as a promising candidate material for cost-effective applications, as it is free from toxic and expensive elements (e.g., indium and gallium).[7–15] To synthesize high-quality a-ZTO thin films, various techniques have been used, including sol-gel,[9] sputtering,[13] pulsed laser deposition,[15] and ALD.[7,14] In particular, ALD provides a precise and conformal control of the atomic concentrations of Zn ([Zn]) and Sn ([Sn]) in the film. By controlling the [Zn]/[Sn] ratio, ALD a-ZTO channels

in thin-film transistors have demonstrated a field-effect mobility up to 13 cm^2/V·s with a large on-to-off ratio of drain current ($>10^9$).[7] Furthermore, controlling the [Zn]/[Sn] ratio allows tunability of conduction-band edge positions, which is also useful for photovoltaic applications by reducing interface recombination and improving device performance.[12,16,17] The significant impact of the [Zn]/[Sn] ratio in a-ZTO thin films on device performance suggests a strong correlation between the atomic structure and electronic transport properties of the films. Because amorphous materials can exhibit a continuum of structures,[18] a probe of local order is needed.

In this work, we investigate the effect of atomic structure in a-ZTO on electron transport properties by using synchrotron-based X-ray absorption spectroscopy (XAS). We perform EXAFS at the Zn and Sn K-edges to probe the local chemical neighborhoods of Zn and Sn atoms in a-ZTO films, respectively. We find that the Debye-Waller factor, which gives a measure of structural disorder,[19] at the Zn *K*-edge increases with increasing [Sn] in the films. The structural disorder is further investigated by XANES analysis, which indicates the amorphization around Zn atoms with increasing [Sn] in the films. Disorder as measured by EXAFS and XANES coincides with a decrease in measured electron mobility, suggesting that the degradation in electron mobility may be correlated with structural changes for Zn rich films ([Zn] > 0.5), whereas for Sn rich regions, larger ionic size of Sn dominates the electron mobility.

A set of a-ZTO thin films is grown on quartz substrates by ALD at a growth temperature of 120 °C. Diethylzinc (DEZ) and a cyclic tin (II) amide ((1,3-bis(1,1-dimethylethyl)-4,5-dimethyl-(4R,5R)-1,3,2-diazastannolidin-2-ylidene)Sn(II))[20] are used as the Zn and Sn precursors, respectively. Hydrogen peroxide (H$_2$O$_2$, 50 wt. %, Sigma Aldrich) is used as the common oxygen source. The compositions of a-ZTO films are

a)Authors to whom correspondence should be addressed. Electronic addresses: siahsincheng@gmail.com and buonassisi@mit.edu
b)S. C. Siah and S. W. Lee contributed equally to this work.
c)Present address: Department of Physics and Division of Energy Systems Research, Ajou University, Suwon 443-749, South Korea.

104, 242113-1

TABLE I. Atomic composition of a-ZTO films measured by RBS and $x = [Sn]/([Sn] + [Zn])$.

Sample	ZnO/SnO$_2$ sub-cycle ratio	Atomic contents			
		[O] (at. %)	[Zn] (at. %)	[Sn] (at. %)	x
Z1T0	1/0	51.8	48.2	0	0
Z3T1	3/1	57.6	33.4	9.0	0.21
Z1T1	1/1	61.7	24.2	14.1	0.37
Z1T3	1/3	65.8	12.2	22.0	0.64
Z0T1	0/1	67.9	0	32.1	1

controlled by varying the sub-cycle ratio of ZnO and SnO$_2$. For example, a sub-cycle ratio of 3/1 involves depositing 3 consecutive cycles of ZnO followed by 1 cycle of SnO$_2$. Pure ZnO and SnO$_2$ films are also deposited by ALD at 120 °C on quartz substrates, respectively. The thickness of all films is ~200 nm to minimize self-absorption issues in XAS measurements. The atomic compositions of the resulting films are measured by Rutherford backscattering spectroscopy (RBS), summarized in Table I.

XAS is performed at the MRCAT Sector 10-ID beamline of the Advanced Photon Source, Argonne National Laboratory (IL, USA). The beamline uses a cryo-cooled Si(111) double-crystal monochromator. In this study, we perform XAS at both the Zn and Sn K-edge transitions, which occur at 9.66 and 29.2 keV, respectively. The thin film samples are measured in fluorescence mode with an incident beam of area $500 \times 500\ \mu m^2$ and a 13-element Canberra germanium solid-state detector with a liquid nitrogen coolant to collect the fluorescence emission. To improve the signal-to-noise ratio, multiple scans are averaged together to achieve effective counts higher than 10^6. The energy scale is calibrated by using the absorption edge of reference metallic Zn or Sn thin films measured simultaneously and the XANES and EXAFS are isolated by normalizing the absorption spectrum and subtracting the smooth atomic background absorption signal from the measured absorption signal using the AUTOBK algorithm in Athena with $R_{bkg} = 1.0$ Å.[21,22] After the background removal, the processed data are transformed from energy space to k-space using the relationship, $k^2 = 2m(E - E_0)/\hbar^2$, where k is the electron wavenumber, m is the electron mass, E_0 is the K-edge absorption energy of the respective elements, and $\hbar$ is Planck's constant. The entire spectrum is weighted by k^2 to compensate for amplitude decay. For further analysis, the k^2-weighted spectra data are Fourier-transformed with a Hanning window as a bandpass filter to enhance the signal-to-noise ratio defined from $k = 1.5$ to 8.0 Å^{-1}.

Fig. 1 shows the resulting Fourier-transformed spectra plotted as the magnitude, $|\chi(R)|$, for both the Zn and Sn K-edges. The first large peak in the spectrum is indicative of the scattering signal from the first nearest neighbor (1NN) shell of atoms.[22] It can also be noted that the amplitudes of $|\chi(R)|$ from higher-order shells ($R > 2$ Å) for all other spectra are strongly attenuated, except for the spectrum collected at Zn K-edge for sample Z1T0 (pure ZnO). This suggests that the higher-order shells around the Zn atoms are well-ordered
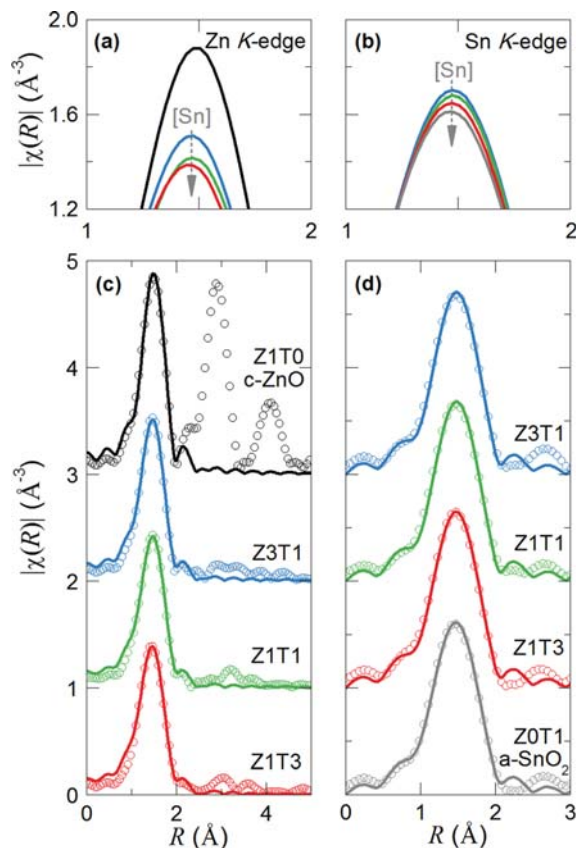

FIG. 1. Fourier-transformed EXAFS spectra at Zn and Sn K-edges. Figures (a) and (b) compare the peak intensity of the 1NN shell at the Zn and Sn K-edges, respectively. The arrows illustrate the decreasing peak intensity with increasing [Sn]. Figures (c) and (d) show the measured (symbols) and fitted spectra (lines) at the Zn and Sn K-edges, respectively (offset for clarity).

in the pure ZnO sample, verifying its crystalline nature. For all a-ZTO and SnO$_2$ films, the EXAFS spectra exhibit limited structure beyond 1NN, indicating a lack of long-range order.

The lack of long-range order in the Z3T1, Z1T1, and Z1T3 samples is consistent with the amorphous structure as characterized by X-ray diffraction measurements we reported elsewhere.[12] Previously, we reported that SnO$_2$ deposited by ALD at 120 °C is nano-crystalline (nc-SnO$_2$).[23] The nc-SnO$_2$ films are grown using a closed-valve mode, during which the nitrogen flow into the reactor was stopped until a base pressure (50 mTorr) was reached, and then a valve between the ALD reactor and the pump was closed during the injection of the Sn precursor.[21] In contrast to these previous results, the SnO$_2$ films in our study are found to be amorphous when made by an open-valve ALD mode without either stopping the nitrogen flow or pumping the reactor down to base pressure between precursor pulses. Furthermore, the saturated growth rate of ~1.2 Å/cycle in the open-valve mode is observed as compared to the slightly increased growth rate of ~1.7 Å/cycle obtained for closed-valve mode growth. We hypothesize that the discrepancy in both crystallinity and saturated growth rate to be due to differences in growth kinetics and highly dependent on precursor's partial pressure during growth. More frequent collisions of the precursor molecules in the closed-valve mode leads to a higher growth rate and makes the film nano-crystalline. Nevertheless, the pure ZnO

films grown with open-valve ALD mode are polycrystalline. These results are verified by XRD measurements (not shown). From Figs. 1(a) and 1(b), it can also be observed that the amplitude of the first shell peak decreases with increasing [Sn].

To gain quantitative structural information for the first shell, we isolate the 1NN peaks from all samples ($1.0 - 2.0\,\text{Å}$ for the Zn K-edge and $1.0 - 2.1\,\text{Å}$ for the Sn K-edge) and fit the peaks using the EXAFS equation given by[24]

$$\chi(k) = S_0^2 \sum_j \frac{N_j f_j(k)}{k R_j^2} e^{-2k^2 \sigma_j^2} e^{-2R_j/\lambda(k)} \sin(2kR_j + \delta_j(k)), \quad (1)$$

where j indicates shells of like atoms, S_0^2 is the passive electron reduction factor, N_j is the coordination number of atoms in the jth shell, k is the photoelectron wavenumber, R_j is the distance to the neighboring atoms, σ_j^2 is the Debye-Waller factor or the mean-squared disorder of neighbor distance, and $\lambda(k)$ is the electron mean free path. The scattering amplitude, $f_j(k)$, and the phase shift, $\delta_j(k)$, are dependent on the atomic number of the scattering atoms. Due to the similarity in the first-shell EXAFS spectra between a-ZTO samples and reference samples, we expect the local structures around the Zn and Sn atoms of the a-ZTO films to resemble those of crystalline ZnO and amorphous SnO_2, respectively. In this case, the 1NNs of Zn and Sn atoms contain only oxygen atoms, thus only the single-scattering paths Zn – O and Sn – O are considered. As starting inputs, the relevant EXAFS parameters for the Zn – O and Sn – O paths are estimated using the crystal structures of ZnO (wurtzite, space group P6$_3$mc)[25] and SnO_2 (rutile, space group P4$_2$/mnm)[26] using the ATOMS and FEFF6 codes implemented in Artemis.[21,27] To reduce the number of fitting parameters, S_0^2 for both Zn (0.84) and Sn (1.00) are obtained by fitting the EXAFS spectra of metallic Zn or Sn thin films collected simultaneously with each sample. Subsequently, non-linear least squares fitting is performed in Artemis to obtain structural parameters like R_j, N_j, and σ_j^2 as summarized in Table II. We obtained R-factors of < 0.01 for all fits.

It can be observed that the bond lengths of Zn – O and Sn – O of all a-ZTO samples have very small changes with respect to composition and are comparable with the reference ZnO and SnO_2. The fitted average bond-lengths, $R_{\text{Zn–O}} \sim 1.98\,\text{Å}$ and $R_{\text{Sn–O}} \sim 2.05\,\text{Å}$, are also in close agreement with previously reported values for wurtzite ZnO[25] and rutile SnO_2.[26] In addition, our fitting results indicate that Zn and Sn atoms have tetrahedral and octahedral

coordination, respectively, as predicted by theoretical calculations.[28,29] This observation is consistent with the oxygen-rich atomic composition measured by RBS, which can be attributed to the use of H_2O_2 as the oxidizing agent.[12,23]

While both R and N have very small changes with Sn content, higher [Sn] leads to an increase in the pseudo-Debye-Waller factor, σ_{Zn}^2 (the subscript is used to denote the respective metal atom) in Zn – O path. The increase in σ_{Zn}^2 can be attributed to an increase in the level of structural disorder surrounding the Zn atoms resulting in a larger spread in the Zn – O bond-length or distortion of the ZnO$_4$ tetrahedra.[19] Furthermore, structural disorder manifests itself as feature changes in the Zn XANES spectra as shown in Fig. 2(a). Such feature changes in the Zn XANES spectra from 9.66 to 9.67 keV are due to a lack of the distinct multiple scattering contributions and have been associated with the amorphization of the Zn chemical environment as observed by Cho *et al.*[30] In addition, isosbestic points observed in Zn-edge XANES as shown in Fig. 2(a) suggest that the local environments of Zn atoms in the three a-ZTO films comprise of a two-phase mixture that is distinctly different from crystalline wurtzite ZnO structure. One plausible explanation of the presence of two phases can be attributed to a segregation of ZnO and SnO_2, which is likely to occur considering the distinct difference in 1NN coordinated oxygen atoms between Zn and Sn. One of the phases could be due to Zn atoms which lie along the interface between the ZnO$_4$ tetrahedron and SnO$_6$ octahedron and experience a different coordination environment whereas the second phase can be due to the Zn atoms located further away from the ZnO/SnO$_2$ interface. On the other hand, an almost constant σ_{Sn}^2 is consistent with almost identical Sn-edge XANES for all samples.

In Fig. 3, the Hall- and field-effect mobilities together with σ^2 of all samples are plotted as a function of cation composition. The field-effect mobilities of a-ZTO are measured by fabricating thin-film transistors with a-ZTO layers as n-channels and more details are reported elsewhere.[7] The Hall mobilities are measured by using the van der Pauw configuration and a magnetic field of 0.75 T. The Z1T1 and Z1T3 samples exhibit too small Hall voltages to measure Hall mobility.[12] In Zn-rich ([Sn]/([Sn] + [Zn]) < 0.5) a-ZTO samples, increasing σ_{Zn}^2 is well-correlated with a decrease in mobility, with respect to increasing [Sn]. The decreased mobility suggests that structural disorder around Zn atoms reduces the film's mobility significantly. In the Sn-rich ([Sn]/([Sn] + [Zn]) = 0.64) a-ZTO sample, on the other

TABLE II. Summary of EXAFS fit parameters for Zn – O and Sn – O bonds. $x = [\text{Sn}]/([\text{Sn}] + [\text{Zn}])$.

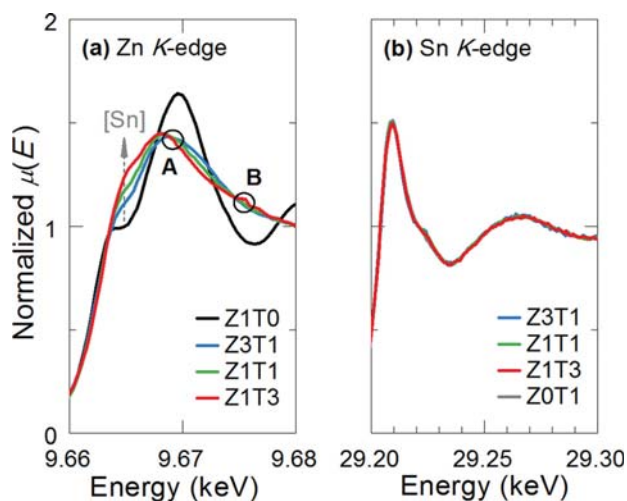|		EXAFS Fit Parameters									
		Zn K-edge					Sn K-edge				
Sample	x	R (Å)	N	σ^2 (Å^2)	E_0 (eV)	R-factor	R (Å)	N	σ^2 (Å^2)	E_0 (eV)	R-factor
Z1T0	0	1.97(3)	3.8(2)	0.002(1)	6.0(8)	0.003	…	…	…	…	…
Z3T1	0.21	1.97(6)	3.7(6)	0.005(1)	4.7(1)	0.002	2.04(7)	5.9(7)	0.006(1)	7.5(6)	0.004
Z1T1	0.37	1.98(1)	3.7(7)	0.007(1)	4.4(3)	0.001	2.04(9)	5.9(1)	0.006(1)	7.4(3)	0.005
Z1T3	0.64	1.98(1)	3.8(9)	0.008(1)	4.0(5)	0.005	2.04(5)	5.8(9)	0.007(1)	7.4(1)	0.003
Z0T1	1	…	…	…	…	…	2.04(7)	5.9(4)	0.007(1)	7.0(7)	0.003

FIG. 2. XANES spectra at (a) Zn and (b) Sn K-edges. The 2 isosbestic points are circled and labelled A and B in (a).

hand, the mobility remains at ~ 0.5 cm^2/V·s with a subtle increase in σ_{Zn}^2.

For AMOS with high ionicity, the conduction band edge typically comprises overlapping Ns orbitals from the metal cations.[1] The isotropic nature of these Ns orbitals causes electron transport to be less sensitive to bonding geometries. However, prior results from other authors on similar material systems such as amorphous ZnO[30,31] (a-ZnO) and amorphous ZnSnO$_3$[32] (a-ZnSnO$_3$) suggest that the conduction band of a-ZTO can comprise of a mixture of Zn-4s and Sn-5s orbitals that are hybridized with O-2p orbitals. In particular, Cho *et al.* have shown from O K-edge XANES that the hybridization strength between Zn-4s and O-2p orbitals in a-ZnO weakens due to structural disorder.[31] In Zn-rich a-ZTO films, the predominant conduction paths are between hybridized Zn-4s and O-2p orbitals. Thus, the reduced mobility by
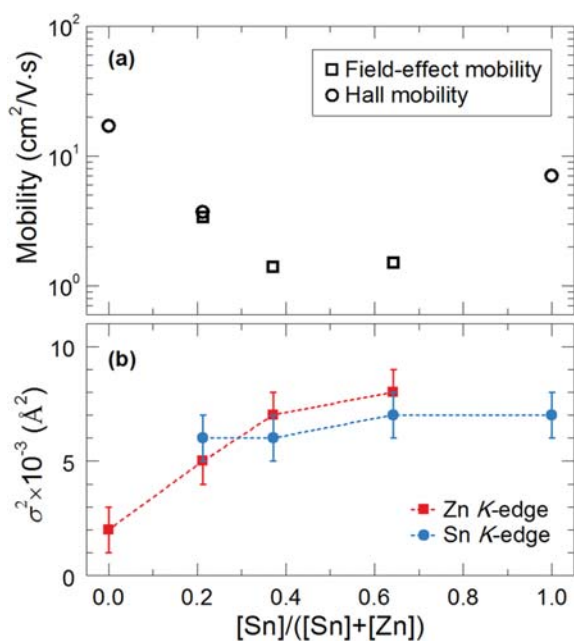
increased [Sn] can be attributed to the structural disorder between Zn and O atoms; reduced hybridization strength of Zn-4s and O-2p orbitals can limit electron conduction pathways.[30,31] On the other hand, Sn-rich a-ZTO films exhibit a very slight increase in the mobilities as [Sn] increases. The dependence of electron mobilities on the composition of the larger metal ion has similarly been observed in Al-Zn-Sn-O[33] and In-Ga-Zn-O[6] systems where the effect has been hypothesized to be due to species with larger ionic radii (Sn^{4+} and In^{3+} ions ($N \geq 5$), respectively) contributing towards conduction. These results suggest that for the Sn-rich a-ZTO film investigated in this work, Sn^{4+} ions which have larger ionic radii thus larger Ns orbital ($N \geq 5$), may begin to dominate electron conduction via Sn-5s – O-2p pathways, thereby increasing electron mobility closer to that of SnO$_2$.

In summary, we use synchrotron-based XAS to investigate the effect of atomic structure of a-ZTO thin films on their electron transport properties. The a-ZTO thin films exhibit higher degree of structural disorder as [Sn] increases in the films. Quantitative EXAFS analysis reveals a strong correlation between σ_{Zn}^2 and electron mobility for Zn-rich films. XANES measurements provide further evidence of structural disorder near Zn atoms in Zn-rich a-ZTO films. The decrease in mobility is correlated with increasing local structural disorder surrounding Zn atoms. Literature reports suggest that the decrease in mobility may be due to reduced hybridization strength of Zn-4s and O-2p orbitals, which may limit electron conduction pathways. Lastly, we observe a slight increase in mobility for the Sn-rich a-ZTO films that can be due to the larger ionic radii ($N \geq 5$) of Sn^{4+} ions.

FIG. 3. Field-effect and Hall-effect mobilities and pseudo-Debye-Waller factors are plotted against [Sn]/([Sn] + [Zn]).

[1]K. Nomura, H. Ohta, A. Takagi, T. Kamiya, M. Hirano, and H. Hosono, Nature **432**, 488 (2004).
[2]T. Kamiya, K. Nomura, and H. Hosono, Sci. Technol. Adv. Mater. **11**, 044305 (2010).
[3]J. K. Jeong, Semicond. Sci. Technol. **26**, 034008 (2011).
[4]M. Orita, H. Ohta, M. Hirano, S. Narushima, and H. Hosono, Philos. Mag. B **81**, 501 (2001).
[5]J. Robertson, Phys. Status Solidi **245**, 1026 (2008).
[6]H. Hosono, J. Non-Cryst. Solids **352**, 851 (2006).
[7]J. Heo, S. Bok Kim, and R. G. Gordon, Appl. Phys. Lett. **101**, 113507 (2012).
[8]P. T. Erslev, E. S. Sundholm, R. E. Presley, D. Hong, J. F. Wager, and J. D. Cohen, Appl. Phys. Lett. **95**, 192115 (2009).
[9]C.-G. Lee, B. Cobb, and A. Dodabalapur, Appl. Phys. Lett. **97**, 203505 (2010).

[10] T. Moriga, Y. Hayashi, K. Kondo, Y. Nishimura, K. Murai, I. Nakabayashi, H. Fukumoto, and K. Tominaga, J. Vac. Sci. Technol. A **22**, 1705 (2004).

[11] H. Q. Chiang, J. F. Wager, R. L. Hoffman, J. Jeong, and D. A. Keszler, Appl. Phys. Lett. **86**, 013503 (2005).

[12] Y. S. Lee, J. Heo, S. C. Siah, J. P. Mailoa, R. E. Brandt, S. B. Kim, R. G. Gordon, and T. Buonassisi, Energy Environ. Sci. **6**, 2112 (2013).

[13] D. Hong, H. Q. Chiang, and J. F. Wager, J. Vac. Sci. Technol. B **24**, L23 (2006).

[14] A. Hultqvist, C. Platzer-björkman, U. Zimmermann, M. Edoff, and T. Törndahl, Prog. Photovoltaics Res. Appl. **20**, 883 (2012).

[15] P. Görrn, M. Sander, J. Meyer, M. Kröger, E. Becker, H.-H. Johannes, W. Kowalsky, and T. Riedl, Adv. Mater. **18**, 738 (2006).

[16] Hultqvist, M. Edoff, and T. Torndahl, Prog. Photovoltaics Res. Appl. **19**, 478 (2011).

[17] S. W. Lee, Y. S. Lee, J. Heo, S. C. Siah, D. Chua, R. E. Brandt, S. B. Kim, J. P. Mailoa, T. Buonassisi, and R. G. Gordon, Adv. Energy Mater. (published online) (2014).

[18] E. Johlin, N. Tabet, S. Castro-Galnares, A. Abdallah, M. I. Bertoni, T. Asafa, J. C. Grossman, S. Said, and T. Buonassisi, Phys. Rev. B **85**, 075202 (2012).

[19] C. J. Glover, G. J. Foran, and M. C. Ridgway, Nucl. Instrum. Methods Phys. Res., Sect. B **199**, 195 (2003).

[20] S. B. Kim, P. Sinsermsuksakul, A. S. Hock, R. D. Pike, and R. G. Gordon, Chem. Mater. **26**, 3065 (2014).

[21] B. Ravel and M. Newville, J. Synchrotron Radiat. **12**, 537 (2005).

[22] B. K. Newman, E. Ertekin, J. T. Sullivan, M. T. Winkler, M. a. Marcus, S. C. Fakra, M.-J. Sher, E. Mazur, J. C. Grossman, and T. Buonassisi, J. Appl. Phys. **114**, 133507 (2013).

[23] J. Heo, A. S. Hock, and R. G. Gordon, Chem. Mater. **22**, 4964 (2010).

[24] D. C. Koningsberger and R. Prins, *X-Ray Absorption: Principles, Applications, Techniques of EXAFS, SEXAFS, and XANES* (Blackwell Scientific Publications, Eindhoven, The Netherlands, 1988).

[25] H. Sawada, R. Wang, and A. W. Sleight, J. Solid State Chem. **122**, 148 (1996).

[26] J. Robertson, J. Phys. C Solid State Phys. **12**, 4767 (1979).

[27] M. Newville, J. Synchrotron Radiat. **8**, 322 (2001).

[28] W. Körner, P. Gumbsch, and C. Elsässer, Phys. Rev. B **86**, 165210 (2012).

[29] J. Lee, Y. Kang, S. Han, C. Seong Hwang, and J.-H. Choi, Appl. Phys. Lett. **103**, 252102 (2013).

[30] D.-Y. Cho, J. H. Kim, and C. S. Hwang, Appl. Phys. Lett. **98**, 222108 (2011).

[31] D.-Y. Cho, J. H. Kim, K. D. Na, J. Song, C. S. Hwang, B.-G. Park, J.-Y. Kim, C.-H. Min, and S.-J. Oh, Appl. Phys. Lett. **95**, 261903 (2009).

[32] J. Lee, D.-Y. Cho, J. Jung, U. Ki Kim, S. Ho Rha, C. Seong Hwang, and J.-H. Choi, Appl. Phys. Lett. **102**, 242111 (2013).

[33] D.-H. Cho, S. Yang, C. Byun, J. Shin, M. K. Ryu, S. -H. K. Park, C.-S. Hwang, S. M. Chung, W.-S. Cheong, S. M. Yoon, and H.-Y. Chu, Appl. Phys. Lett. **93**, 142111 (2008).